ICN – A Treasure Mine of Non-Covalent Interactions: A Matrix Isolation FTIR and *Ab Initio* Study

Amala Raj

A dissertation submitted for the partial fulfilment of BS-MS dual degree in Science

Indian Institute of Science Education and Research Mohali

April 2018

Certificate of Examination

This is to certify that the dissertation titled "ICN – A Treasure Mine of Non-Covalent Interactions: A Matrix Isolation FTIR and Ab Initio Study" submitted by Amala Raj (Reg.No: MS13068) for the partial fulfilment of BS-MS dual degree programme of the institute has been examined by the thesis committee. The committee finds the work done by the candidate satisfactory and recommends that the report be accepted.

Dr. P. Balanarayan   Dr. Arijit Kumar De   Dr. Sugumar Venkataramani

Prof. K. S. Viswanathan

Dated: 20 April, 2018

Declaration

The work presented in this dissertation has been carried out by me with Prof. K. S. Viswanathan at the Indian Institute of Science Education and Research Mohali. This work has not been submitted in part or full for a degree, a diploma, or a fellowship to any other university or institute. Whenever contributions of others are involved, every effort is made to indicate this clearly, with due acknowledgment of collaborative research and discussions. This thesis is a bonafide record of original work done by me and all sources listed within have been detailed in the bibliography.

Amala Raj

MS13068
(Candidate)
Dated: 20 April, 2018

In my capacity as the supervisor of the candidate's project work, I certify that the above statements by the candidate are true to the best of my knowledge.

Prof. K. S. Viswanathan

(Supervisor)

Acknowledgements

List of Figures

List of Tables

CONTENTS

ABSTRACT

Non-covalent interactions are molecular interactions that involve dispersion type interactions between the interacting species. Although the energies of non-covalent interactions are very small compared with that of a covalent bond, the cooperative nature of non-covalent interactions make them significant in determining supramolecular architectures. One of the interesting types of non-covalent interactions is the halogen bond. In order to experimentally observe the halogen bond, cyanogen iodide (ICN) was chosen for the study, as this molecule allows for the manifestation of a strong iodine bond. The electrostatic potential map of ICN shows the presence of halogen bonding, hydrogen bonding and carbon bonding sites in it. The ICN molecule can therefore, manifest an iodine bond, a hydrogen bond and a carbon bond.

Matrix isolation infrared spectroscopy is a powerful tool to study non-covalent interactions. Negligible intermolecular interactions and elimination of Doppler and collisional broadening give rise to sharp peaks, which enables us to study features of weakly bound complexes.

In this thesis, non-covalent interactions in ICN-water and ICN-methanol complexes were studied both experimentally and computationally. Calculations were carried out in the M06-2X/DGDZVP level of theory.

CHAPTER 1: INTRODUCTION

Non-covalent interactions are molecular interactions that do not involve sharing of electrons, but rather involve dispersion type interactions between the interacting species. Although the energies released in the formation of non-covalent interactions are very small compared with that of a covalent bond, the cooperative nature of non-covalent interactions make them significant in determining supramolecular architectures. Non-covalent interactions come in many hues and colors, such as hydrogen bonds, halogen bonds, π-π stacking, etc.

1.1 HYDROGEN BOND

Of the non-covalent interactions, the most discussed example is that of the DNA molecule, in which the two strands of DNA are held together by hydrogen bonds that occur between complementary nucleotide base pairs. **"The hydrogen bond is an attractive interaction between a hydrogen atom from a molecule or a molecular fragment X–H in which X is more electronegative than H, and an atom or a group of atoms in the same or a different molecule, in which there is evidence of bond formation"**.[1] It is an electrostatic dipole-dipole interaction between donor and acceptor atoms. The hydrogen acceptor has to be a strongly electronegative atom or an electron cloud. A hydrogen bond can occur between two molecules or within a single molecule. If the bond is between molecules, then it is an intermolecular hydrogen bond. Intermolecular hydrogen bonding is responsible for the high boiling point of water compared to other hydrides of group 16 have much weaker hydrogen bonds. An intramolecular hydrogen bond occurs within a single molecule. Hydrogen bonding between base pairs of DNA is an example of intramolecular hydrogen bonding. In most of the cases, the X-H bond length of donor increases on hydrogen bond formation. Therefore, the X-H frequency shows a red shift in the vibrational spectrum.

1.2 HALOGEN BOND

"A halogen bond occurs when there is evidence of a net attractive interaction between an electrophilic region associated with a halogen atom in a molecular entity and a nucleophilic region in another, or the same, molecular entity".[2] Halogen bonding is a non-covalent interaction between a halogen atom X in a molecule with negative sites, such as a lone pair of Lewis base or π cloud in others (R-X---: B). In most cases, the R-X-B angle is nearly

180^0. Halogen bonding occurs in various biological systems. Halogen bonding (I···O) plays a significant role in the recognition of thyroid hormone, which is naturally iodinated.[3] Because of its high directionality, halogen bonding can play a vital role in drug design and crystal engineering.

The surprising aspect of a halogen bond is that the halogen atoms, viewed as having negative charges, are acting as electron acceptors. The reason for such an interaction is the presence of a positive electrostatic potential region in front of the halogen atom along the C-X axis in the molecule R-X. This positive region is called the **σ hole**, and it makes the halogen atom an electron acceptor (Fig 1).

-0.009 a.u.

σ-hole

+0.054 a.u.
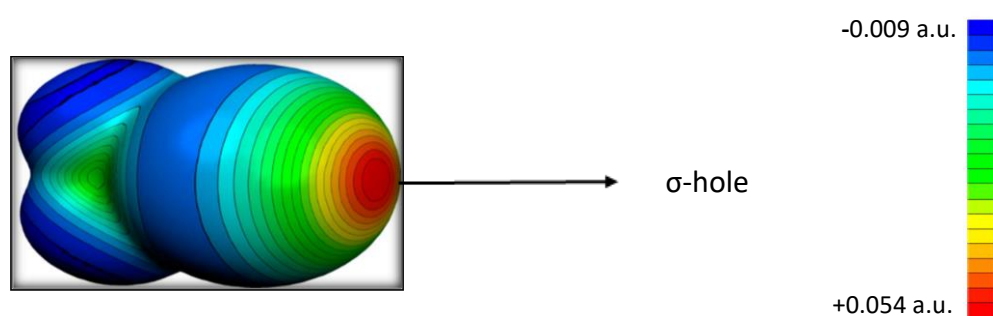
Figure 1: Molecular Electrostatic potential of CF₃I

Population analysis performed on molecules CF_3X, where X is F, Cl, Br or I, showed that the three unpaired electrons on Cl, Br and I produce a negative electrostatic potential around halogen, which makes the outer most region along R-X axis positive.[4] This region of positive potential, which is formed due to anisotropy of charge distribution is the σ hole. The strength of halogen bonding varies based on the magnitude of σ hole, which in turn depends on the relative electronegativity of the halogen atom with respect to the rest of the molecule. Fluorine atom being strongly electronegative does not show halogen bonding since there is an influx of electron density which can neutralize the σ hole. A σ hole is observed in case of CF_3I and not in CH_3I. In CH_3I the remainder of the molecule donates electron density to the σ hole whereas, in CF_3I, the Fluorines withdraw electron density towards it making the σ hole on Iodine more positive. The strength and size of the positive potential region increases in the order Cl< Br< I. Iodine halogen bonding with maximum strength because of its lower electronegativity compared to other halogens (fig. 2).

CF4

CF3Cl

CF3Br

CF3I

−0.009 a.u.

+0.054 a.u.
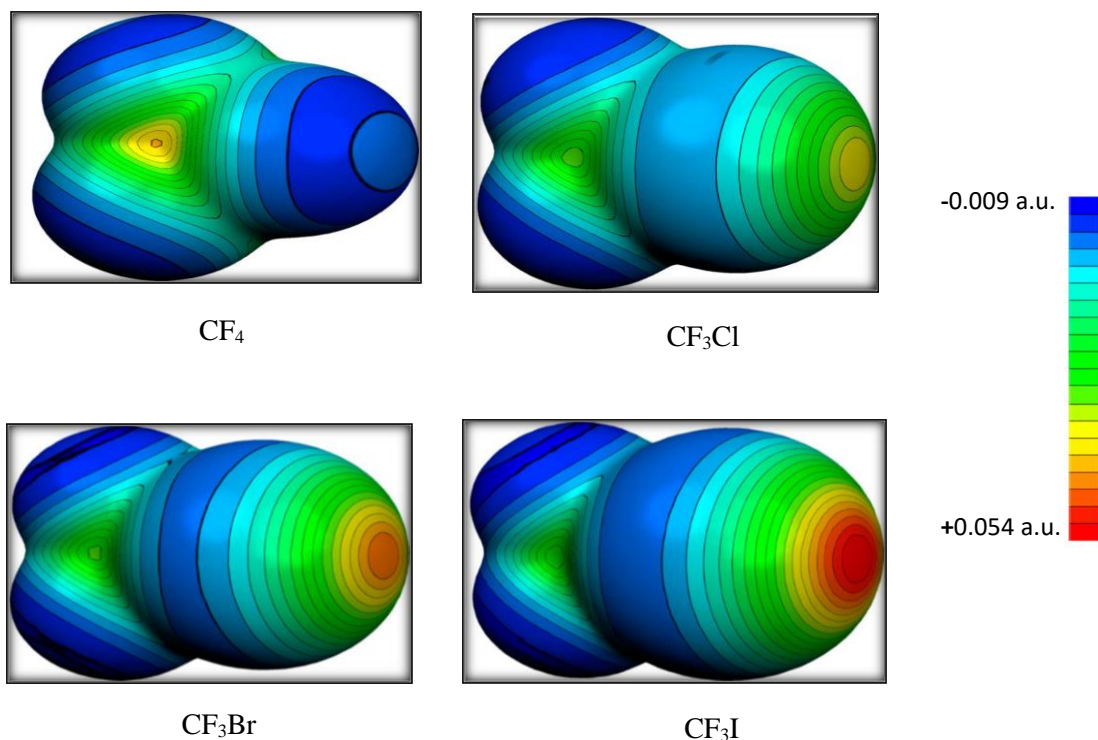
Figure 2: Comparison of σ-hole in CF₃X, where X= F, Cl, Br or I

It has been shown previously that halogen bond can coexist[5,6], compete[7,8]or cooperate[9] with the ubiquitous hydrogen bond in some systems. In the crystal structure of trichloroacetic acid, Cl···O bond is observed together with O···H interaction[2] (fig. 3).
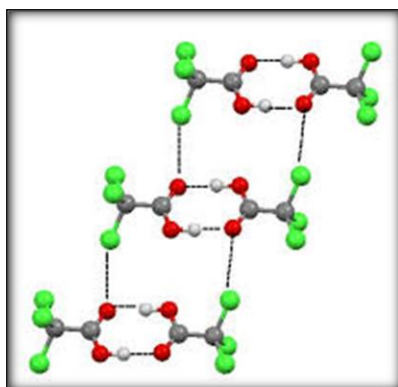
Figure 3: Crystal structure of Trichloroacetic acid (broken lines show H···O and Cl···O contacts)

A specific self-assembly process of 1,1,3,3-tetra-oxo-2-bromo-4,4,5,5,6,6-hexafluoro-1,3-dithiacyclohexane and 2-methyl pyrazine is driven by coexisting halogen bonding and hydrogen bonding.[8] *Ab initio* studies showed the possibility of halogen bonding (X$\cdots$O) and hydrogen bonding (H$\cdots$O) interactions in the complexes between hypohalous acids (HOX, X= F, Cl, Br) and formaldehyde.[10] It was confirmed that hydrogen bonding was favored over the halogen bonding and the difference in strengths of both decreases when the size of halogen increases. Cooperative nature of halogen bonding and hydrogen bonding in XY$\cdots$HNC$\cdots$XY where, (X, Y = Br, F, Cl) is also reported in the literature.[11] It was shown that hydrogen and halogen bond stabilization energies in the trimers were more compared to that of individual dimers (HNC$\cdots$XY and XY$\cdots$HNC), indicating that both the interactions are enhanced.

1.3 CARBON BOND

Another type of a non-covalent interaction is the carbon bond, in which an electron deficient carbon atom is bound to an electron-rich center in another molecule. Electrostatic potential calculations on methane show the presence of four equivalent maxima on the four tetrahedral faces with negative ESP values. When one of the hydrogen atoms in methane is substituted with an electronegative group such as –OH or –F, the CH_3 tetrahedral face shows an electrostatic maximum with a positive ESP value.[12] Due to the presence of a positive potential region, this face can act as an electron density acceptor, thereby forming a non-conventional Carbon bond. Methanol and Fluoromethane can also act as hydrogen bonding acceptor sites due to the presence of F and O. Therefore, the same molecule can show carbon bonding and hydrogen bonding. Arunan *et al.*[12] have shown that the CH_3 face in methanol and Fluoromethane can interact with electronegative atoms to form complexes like $H_2O\cdots CH_3X$, $H_2S\cdots CH_3X$, $HY\cdots CH_3X$, $LiY\cdots CH_3X$, $H_3N\cdots CH_3X$, $H_3P\cdots CH_3X$, where Y = F, Cl, Br and X =OH, F. It was also shown that carbon bonding can play a significant role in hydrophobic interactions since the electronegative atom is binding to a hydrophobic center (fig. 4).

A comparison of group 14 and group 17 σ holes in F_3MX molecules was performed by Politzer *et al.*[13] where M is C, Si or Ge and X is F, Cl, Br or I. Group 14 σ hole is observed in all these molecules and group 17 σ hole is observed in all molecules except when X=F. The strength of σ holes of M and X increased in going from lighter to a heavier atom in a given group. The interaction of σ holes with a lone pair of HCN was studied by this group. It was shown that when M=C, for X= Br and I, the global minimum is the halogen bonded structure. For X=F, both halogen and carbon bonded structures have comparable interaction energies.

But, when M=Si/Ge the carbon bonded complex is shown to be more stable than the halogen bonded complex.
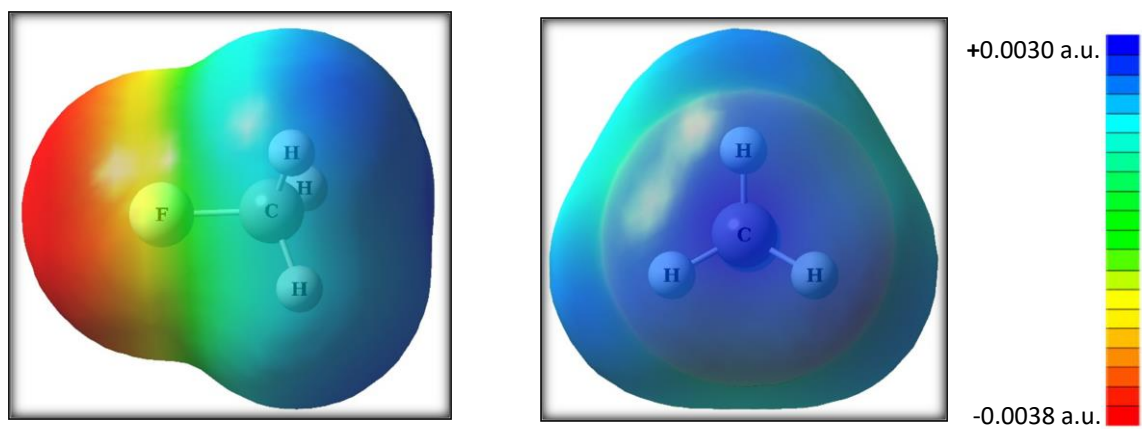
Figure 4: Electrostatic potential surface of Fluoromethane

CHAPTER 2: EXPERIMENTAL PROCEDURE

2.1 MATRIX ISOLATION FTIR SPECTROSCOPY

Matrix isolation spectroscopy is a technique that has been popularly used for the study of weakly bound complexes, reactive intermediates, short-lived species, and conformations of molecules[14,15]. The technique involves trapping of molecules in a rigid cage of an unreactive host material (the matrix) at cryogenic temperatures (~10 K) (fig. 5). The technique was first proposed by Pimental for the study of reactive species.

Gas phase   **Matrix isolation**

Sample molecule   Matrix gas
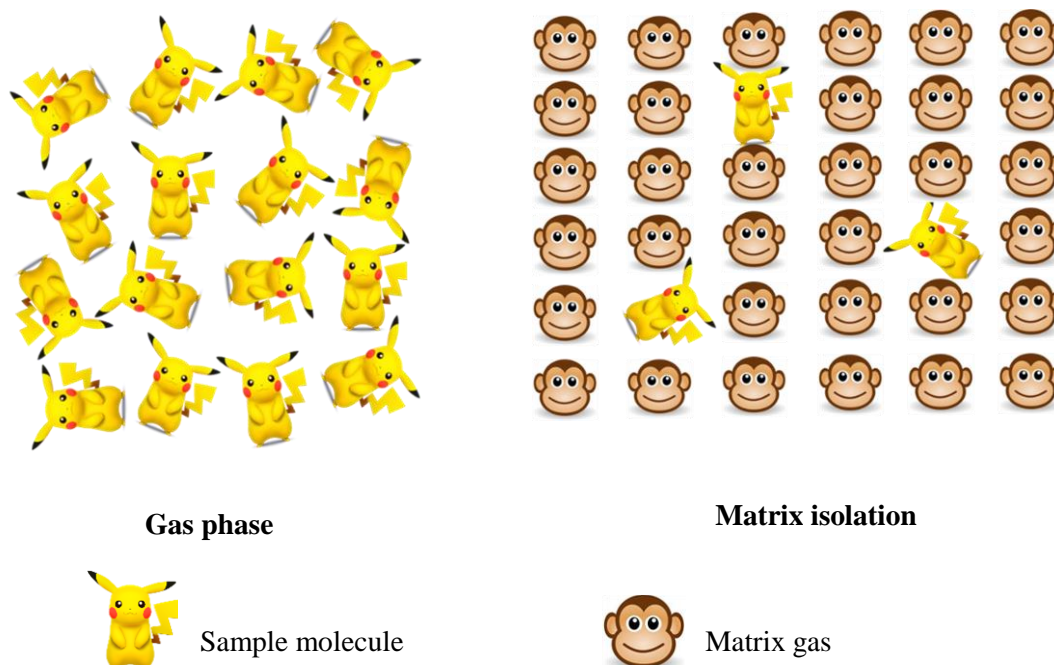
Figure 5: A schematic showing Matrix Isolation of sample molecules

In the technique of matrix isolation, the molecule of interest is mixed with a large excess of an inert gas such, as Ar or N_2, which serves as the matrix gas. The gas mixture is effused into a vacuum system and is condensed onto a cold surface, maintained at ~10 K, to ensure rapid solidification. A large matrix to substrate ratio (1000:1) is maintained so that the molecules of interest are well separated from each other and do not interact with each other. The isolation is further ensured as the rigidity of the matrix cage prevents diffusion of molecules at the low temperature $(\sim 10 K)$. and also reduces the chances of any possible internal rearrangements. The maintenance of low temperature requires cryogenic technology, and the

high vacuum techniques. High vacuum condition ($\sim 10^{-6}$mmHg) is also necessary to ensure that the deposited matrix is free from contamination.

Matrix isolation is combined with various spectroscopic methods to probe the trapped molecules. The most popular spectroscopic techniques used to study the matrix-isolated species are infrared spectroscopy, electron spin resonance spectroscopy, electronic spectroscopy and fluorescence spectroscopy. Matrix Isolation Infrared spectroscopy is widely used to study weakly bound complexes formed in the matrix.

2.2 ADVANTAGES OF MATRIX ISOLATION

The main advantages of the matrix isolation technique is that the spectral features exhibit considerably smaller linewidths compared to gas, liquid or solid phase spectrum. The large matrix to sample ratio prevents intermolecular interactions between the molecules of interest. Therefore, collisional broadening is considerably reduced. Also, the low temperature and rigidity of the matrix eliminate Doppler broadening. Furthermore at the temperature of the matrix, only the lowest rovibrational and electronic levels are populated, which results in a simple spectrum involving only a few states, which is often referred to as spectral decongestion.

2.3 PROPERTIES OF MATRIX

- It must be chemically inert and free of any absorption at the spectral region of interest that would interfere with the detection of isolated molecules.

- It should be easily available with a high degree of purity. Argon and nitrogen are readily and cheaply available, obtained by fractional distillation of air.

- It must have sufficient vapour pressure at room temperature to allow deposition of analyte molecules.

- It should form non scattering matrixes.

2.4 STRUCTURE OF MATRIX

A single crystal model is generally used for analysis of possible sites available for a matrix isolated molecule. Argon crystallises in face centred cubic structure (cubic close-packed) whereas nitrogen adopts hexagonal close packing. Each atom is surrounded by 12 nearest neighbours. Possible occupational sites in these close-packed lattices are interstitial and substitutional sites. In both hcp and ccp, only 74% of the lattice is occupied, leaving 24%

unoccupied. These interstitial sites can be occupied by matrix isolated atoms. Due to the small size of an interstitial site, only monoatomic positive ions are likely to occupy these sites.

In a substitutional site, a matrix atom is replaced by a substrate molecule. Depending on their size and shape, a matrix isolated molecule can occupy multiple substitutional sites. The removal of one atom from the lattice of the matrix gives a single substitutional site with 12 nearest neighbours. The removal of 2 adjacent atoms leaves a site with 18 nearest neighbours. As more and more matrix atoms are replaced, the size of the cage increases.

It is important to consider how isolated the analyte molecules are inside a matrix since their aggregation can lead to changes in the spectrum. If a substrate is occupying one substitutional site, then the probability of not finding another substrate near to it is given as,

$$p = 1 - 12r$$

Where, r is the reciprocal of matrix ratio. A matrix ratio of 1:1000 gives an effective isolation of 99%. To trap a larger molecule in a cage containing 122 matrix atoms,

$$p = 1 - 122r$$

To ensure 99% isolation, a matrix ratio of 1:10000 is required.

2.5 RIGIDITY OF MATRIX

The matrix should remain rigid to prevent any diffusion of molecules. A rule-of-thumb is that a matrix can be considered rigid below 30% of its melting point. At this temperature, the matrix rearranges towards the most stable crystal form, during which time, weak interactions between trapped species can occur.

2.6 MATRIX EFFECTS

Ideally, the matrix should be inert towards the trapped species. In reality, the matrix atoms interact with the isolated species in a variety of ways resulting in perturbations in the spectral features. These matrix effects can be identified in a spectrum as a shift in the peak positions, peak multiplets and broadening of peaks.

The popularly used matrix gases like argon and nitrogen cause small perturbations (<1%) in the vibrational features from the gas phase values of molecules. These frequency shifts arise from the electrostatic, dispersive, inductive and repulsive interactions of sample molecules with the matrix.

Sample molecules may be trapped in sites with different environments. The spectral features of the matrix-isolated species are perturbed depending on the environment of the site in which they are trapped, thereby resulting in multiple spectral features. This is called *site effect*. In some cases, these multiplets are not completely resolved which leads to broadening of peaks. During annealing, the trapped species can sometimes move from an unstable site to a stable one, which may result in the disappearance of the multiplets. The presence and the structure of the multiplet, will not be the same in different matrix gases. Hence experiments are usually performed in at least two different matrices, to identify matrix site effects.

When small molecules are trapped in a matrix, quantized rotational motions are possible corresponding to which additional spectral features will be observed. Multiplets due to rotational effects can be distinguished from site multiplets based on temperature effects. Multiplets due to the rotational effects, show reversible changes as the temperature of the matrix is cycled, while multiplet features due to site effects are usually irreversible. Faster deposition can lead to low concentration of impurities. Splitting due to impurities will vary with the matrix ratio, which can be used to discern effects due to impurities.

When the concentration of substrate is increased, molecular aggregates such as dimers, trimers and other multimers can be formed in the matrix. By varying the concentration of the sample, features molecular aggregates can be identified.

2.7 MATRIX ISOLATION FTIR SETUP

2.7.1 Vacuum system

A two-stage pumping system with a rotary pump backing a silicon oil-diffusion pump to give an ultimate pressure of 10^{-6}mmHg. An Edwards Diffstak MK2 series diffusion pump is used which has a pumping speed of ~ 280L/sec for air. The backup rotary pump has a capacity of 300L/min. The base vacuum obtained is 10^{-6} mmHg at room temperature and 10^{-7} mmHg at 12K. The diffusion pump is cooled using chilled water obtained using a 3kW chiller.

2.7.2 Cryostat

The major components of the closed cycle cryostat are the cold head, compressor, vacuum shroud and radiation shield. The Gifford-McMahon refrigeration cycle takes place in the cold head. It is connected to the He compressor by two gas lines and an electrical cable. One of the gas lines supplies high pressure He to the cold head and the other returns low pressure He from the cold head. The vacuum shroud surrounds the cold head and reduces the heat load due to conduction and convection.

2.7.3 Mixing chamber

A stainless steel mixing chamber of 1 Litre capacity is used to mix the matrix and analyte molecules in the desired ratio.

2.7.4 Matrix gas

Argon and nitrogen matrix gases are used for the experiments.

2.7.5 FTIR spectrophotometer

The FTIR spectra of molecules isolated in the matrix were recorded using a Bruker Tenor 27 FTIR spectrophotometer. It is operated at a resolution of $0.5 cm^{-1}$. Typically 8 scans are recorded to obtain a good signal-to-noise ratio. A Globar (heated silicon carbide) source is used to obtain the spectral region from 400-4000 cm^{-1}. A heater-temperature controller unit is used to maintain the matrix at required temperatures above 12 K. The home built matrix isolation FTIR setup is shown in fig. 6.
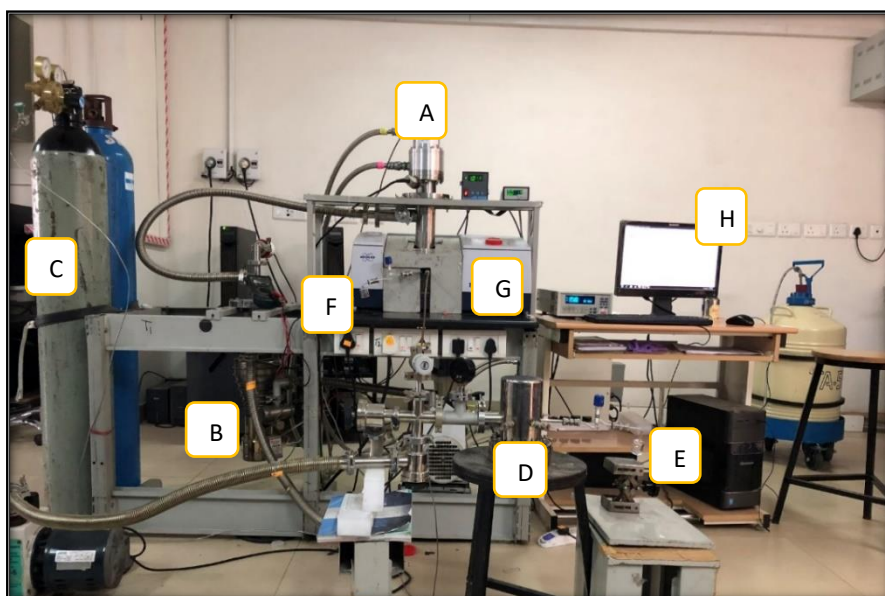
A	Cryostat
B	Diffusion pump
C	Matrix gas cylinder
D	Mixing chamber
E,F	Sample holders
G	FTIR spectrometer
H	Data acquisition

Figure 6: Matrix Isolation FTIR homebuilt setup

2.8 EXPERIMENTAL PROCEDURE

Before starting the experiment it was made sure that the vacuum in the system is in the realm of 10^{-6}mmHg. The sample bulb was thoroughly degassed before loading the sample. The sample was loaded inside a glove box to remove moisture and other impurities. It was subjected to several freeze-pump-thaw cycles before deposition. The sample was equilibrated at a

required temperature (to obtain desired vapour pressure), for about an hour. The desired matrix to sample ratio was maintained by controlling the vapour pressure of the sample. The desired vapour pressure was obtained by maintaining the sample at the appropriate temperatures using liquid nitrogen. The appropriate temperatures were calculated using the Clausius-Clapyron Equation.

$$ln\frac{P_2}{P_1} = \frac{\Delta H}{R}\left(\frac{1}{T1} - \frac{1}{T2}\right)$$

Where P_1 and P_2 are the vapour pressures at temperature T_1 and T_2 respectively and ΔH is the heat of vaporization.

The samples were equilibrated at an appropriate temperature for about an hour. A double jet experiment was performed, where the matrix (argon) and sample were allowed to deposit on the cold KBr window through two different valves. The rate of deposition was controlled using a fine needle valve which was set at a value of 230.

Once the sample and matrix are deposited at 12 K, the spectrum of matrix-isolated species is recorded. The temperature is then raised to 32 K (30% of melting point for argon) and the Matrix is held at this temperature for 30 minutes. Possible internal rearrangements and weak intermolecular interactions take place in the matrix at this stage. The matrix is then cooled back to 12 K and a spectrum is recorded again. This process is called *annealing*.

CHAPTER 3: COMPUTATIONAL METHODOLOGY

Quantum chemical calculations were performed using Gaussian 09 suite of programmes[20], to support the experimental results on various non-covalent interactions under consideration, Properties such as structure, energy, atomic charges and vibrational frequencies were analyzed for the monomers and complexes. AIM[21] software was used to confirm the presence of non-covalent interactions. NBO analysis was carried out to understand the donor and acceptor orbitals involved in these interactions.

3.1 GEOMETRY OPTIMIZATION

Geometry optimization is a procedure to determine the minimum energy structure of a molecule. A guess molecular structure is provided as an input. The energy and gradient of energy are then computed at the point on the potential energy surface corresponding to the initial geometry. This information is used to determine in which direction the next step is to be taken to improve the geometry. An optimized geometry is obtained at the minimum of the potential energy surface. At the stationary point, the gradient of energy will be zero. A stationary point can be a minimum, maximum or a saddle point. For a minimum (optimized geometry) all frequencies are real.

For complexes with an iodine atom, DGDZVP basis set was used for the calculations. For systems without an iodine atom, aug-cc-pVDZ basis set was used. Optimization was carried out at the M06-2X and MP2 levels of theory.

3.2 INTERACTION ENERGY OF THE COMPLEX

The interaction energy of a complex is given by

$$\Delta E = E_{AB} - E_A - E_B$$

Where E_A, E_B, and E_{AB} are the computed energies of monomers A, B, and complex AB respectively.

If the complex is more stable relative to the monomers, the interaction energy will be negative. The interaction energy of the complex was corrected for zero point energy (ZPE) and the basis set superposition error (BSSE).[16] ZPE and BSSE corrections were not simultaneously performed as this procedure is known to overcorrect the stabilization energy. [17]

3.3 VIBRATIONAL FREQUENCIES

Frequency calculations were performed for all the optimized geometries. The gradient of potential energy at minimum gives the force constant, k. The relation between force constant (k) and vibrational frequency of a normal mode (υ) is given by the equation,

$$\upsilon = \sqrt{\frac{k}{\mu}}$$

Where, μ is the reduced mass.

It was ensured that all frequencies are real at the stationary point, which indicates that the geometry indeed corresponded to a minimum. The calculated vibrational frequencies were used to assign the spectral features observed in the matrix isolation experiments. In particular, frequency shifts of the modes in the complex, relative to frequencies of the same mode in the submolecules, were calculated.

3.4 ATOMS IN MOLECULES (AIM) ANALYSIS

Atoms in molecules (AIM) theory, which is based on the analysis of electron density topology in a molecular system, was first proposed by Bader. To perform the AIM analysis, the wave function corresponding to the optimized geometry of a complex is generated using Gaussian 09 suit of programmes. The wave function is then used to generate an electron density plot of the complex. The electron density plot yields bond critical points, charge density ρ and gradient of the charge density $\nabla^2\rho$ (which is defined as the sum of eigen values of Hessian matrix, i.e. $\lambda_1 + \lambda_2 + \lambda_3$). The charge density $\rho(r)$ is a physical observable which has a definite value at each point in space. At a bond critical point the first derivative of $\rho(r)$ vanishes. It can be a maximum, a minimum or a saddle point. The sign of second derivative of $\rho(r)$ determines whether it is a maximum or minimum.

The number of non-zero curvatures of ρ at the critical point is called the rank of the critical point (ω). The algebraic sum of signs of these eigen values is the signature of the critical point (σ). A critical point can be labelled as (ω,σ). For example, a (3,-1) critical point means 3 non-zero curvatures from which 2 are maxima and one is a minimum. This corresponds to a bond between two atoms. A (3,+1) critical point is a ring critical point, while a (3,-3) critical point corresponds to a cage critical point.

The charge density, ρ together with $\nabla^2\rho$, provides information about how charge density is distributed around the bond critical point. For closed shell interactions, as found in ionic,

hydrogen-bonded, and van der Waals molecules, $\nabla^2\rho$ should be positive. The criteria for the existence of hydrogen bonding were given by Koch and Popelier.[18] According to the criteria, the H-bonds should have an electron density at the bond critical point in the range 0.002−0.034 au and $\nabla^2\rho$ within 0.024−0.139 au. For halogen bonding an electron density at the bond critical point is in the range 0.011-0.040 au and $\nabla^2\rho$ is within 0.043-0.121 au.[19]

3.5 NATURAL BOND ORBITAL ANALYSIS

NBO analysis is performed to identify the orbitals involved in a bonding interaction. In an NBO analysis, a given wave function is transformed into a localized form, corresponding to a Lewis structure. The input atomic orbital basis set is transformed via natural atomic orbitals (NAOs) and natural hybrid orbitals (NHOs) into a set of natural bond orbitals (NBOs). The natural bond orbitals obtained in this way correspond to the widely used Lewis picture, in which two-centre bonds and one-centre lone pairs are localized. The localized orbitals in the Lewis structure can interact strongly with each other. An empty orbital can act as an acceptor and a filled bonding or lone pair orbital can act as a donor. These interactions can strengthen and weaken the bonds. Electron delocalizations in the Lewis structure depicts donor-acceptor interactions.

Calculations are performed by examining all the possible interactions between donor NBOs and acceptor NBOs. Second order perturbation theory is used to calculate the energy of each interactions. Since these interactions lead to loss of occupancy of electron density from a localized NBO of the ideal Lewis structure into an empty non-Lewis, they are referred to as `delocalization corrections' to the natural Lewis structure. The extent of delocalization of electron density depends on the relative energy of orbitals and the orbital symmetry of donor and acceptor. To understand the orbitals involved in the non-covalent interactions, the delocalization interactions between the monomers are considered.

CHAPTER 4: RESULTS AND DISCUSSIONS

One of the interesting types of non-covalent interactions is the halogen bond. Amongst the halogens, Iodine forms the strongest halogen bonds. In order to experimentally observe the halogen bond, cyanogen iodide (ICN) was chosen for the study, as this molecule allows for the manifestation of a strong iodine bond. In this molecule, iodine is attached to CN- which is a strong electron withdrawing group which can enhance the strength of σ-hole associated with iodine (Fig. 7).
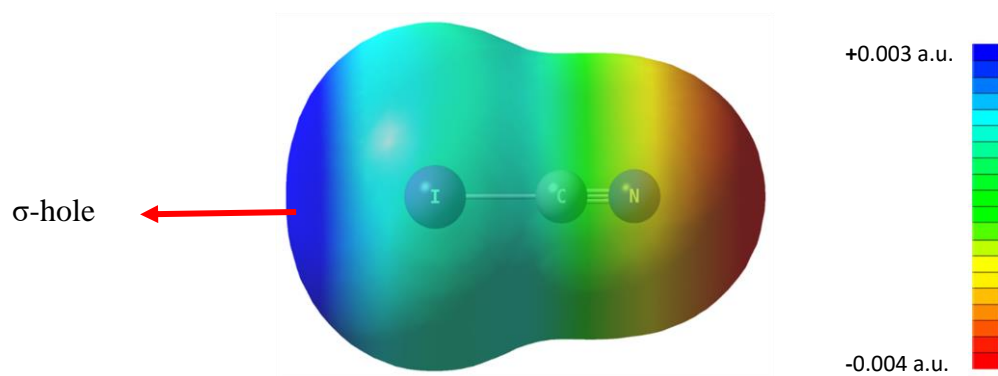
Figure 7: Molecular electrostatic potential of ICN at the MO6-2X/DGDZVP level of theory

The electrostatic potential map of ICN shows the presence of σ hole in front of iodine which can act as an electron accepting site. In addition, there is also a region of a negative electrostatic potential, associated with the nitrogen, which can act as a proton acceptor site, giving rise to the possibility of a classical hydrogen bond. The ICN molecule can therefore, in principle, manifest both an iodine bond and a hydrogen bond (Fig 8).
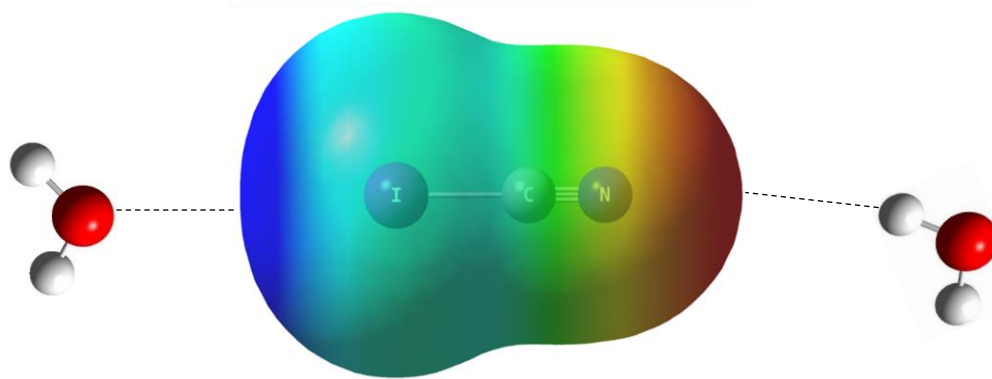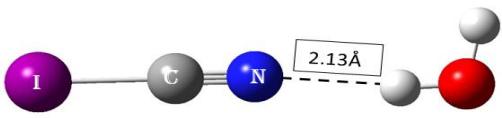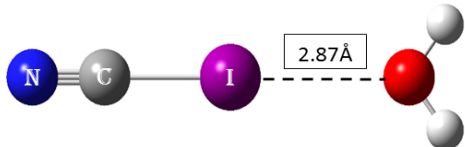
Figure 8: Molecular electrostatic potential of ICN and possible interactions

4.1 ICN-WATER COMPLEXES

      To understand halogen bonding and hydrogen bonding interactions in ICN, complexes of ICN with water were studied. Quantum chemical calculations were performed using Gaussian 09 suite of programmes, at the M06-2X/DGDZVP level. The basis set was so chosen to accommodate iodine in the calculations. The different isomers of $ICN\cdots H_2O$ computed at this level are given below along with the Raw, ZPE and BSSE corrected stabilization energies of the complex in table 1.

Table 1: Optimized geometries of ICN-water system and the interaction energies of complexes

Isomer	Interaction Energy Raw/ZPE/BSSE (kcalmol^{-1})
Hydrogen bonding	-4.5/-3.3/-3.8
Halogen bonding	-8.2/-7.2/-7.6

      It can be seen that three types of non-covalent interactions are shown in this system; a halogen bonded complex involving an $I\cdots O$ interaction, a classical hydrogen bonded interaction between N of ICN and H of H_2O. In addition, there was also a carbon bonded complex, which can be manifested as a $C\cdots O$ interaction. Of these isomers, the halogen bonded isomer is the most strongly bound complex, with a BSSE corrected interaction energy of -7.6 kcal/mol. The hydrogen bonded complex was next in stability with a BSSE corrected interaction energy of -3.8 kcal/mol. The carbon bonded complex also had an interaction energy similar to the hydrogen bonded complex. Clearly, the iodine bonded complex is the global minimum on the potential energy surface. In the halogen bonded isomer, $I\cdots O$ bond length is 2.87 Å and the C-I-O angle is nearly equal to 180^0. In the hydrogen bonded complex $N\cdots H$ bond length is equal to 2.13 Å and N-H-O angle is equal to 171^0.

4.1.1 AIM Analysis

The charge density topology of molecules was studied by applying the AIM theory by Bader to the optimized geometries. Using the theory bond critical points (3,-1) associated with the complexes were located. The structures obtained at the M06-2X/DGDZVP level of theory are shown in fig 9. The bond critical points corresponding to the halogen and hydrogen bonds have been circled.

Hydrogen bonded complex

Halogen bonded complex
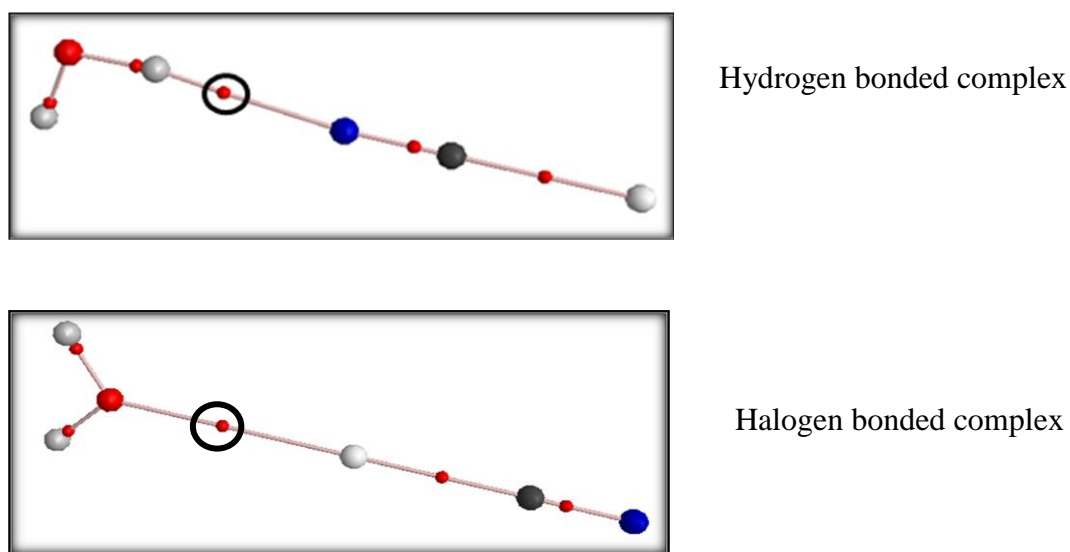
Figure 9: Structures of the complex showing bond critical points at the M06-2X/DGDZVP level of theory

We also computed the electron density $\rho(r)$ and Laplacian of the electron density at the bond critical points corresponding to the intermolecular non-covalent interactions, the values of which are given in Table2.

Table 2: AIM data for the different isomers of ICN-water complex

Isomer	Charge density at b.c.p. $\rho(r)$	Laplacian of $\rho(r)$ at b.c.p.
Halogen bonded complex	0.018 a.u.	0.068 a.u.
Hydrogen bonded complex	0.017 a.u.	0.066 a.u.

The values of $\rho(r)$ and Laplacian of $\rho(r)$ at bond critical points are in good agreement with the values given in literature for halogen bonding[19] and hydrogen bonding[18].

Frequency calculations were also performed at the MO6-2X/DGDZVP level of theory. The vibrational frequencies corresponding to different normal modes of the optimized structures were calculated. All the vibrational frequencies were positive indicating that the obtained geometries were indeed minima on the potential energy surface.
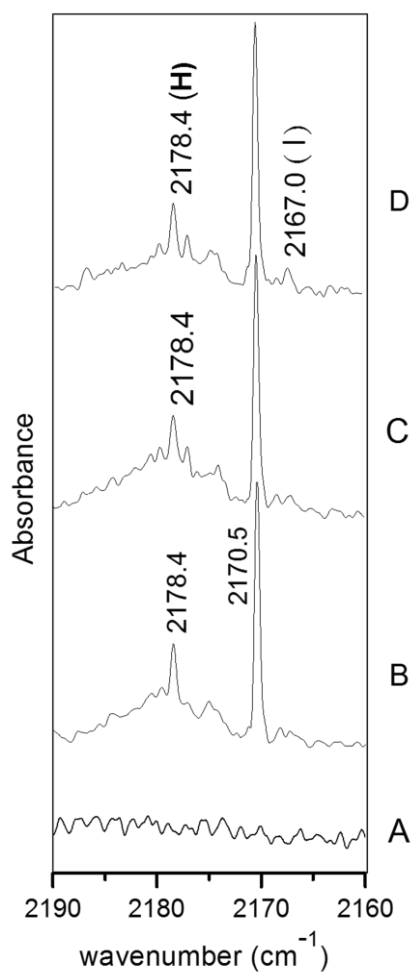
4.1.2 Experimental

ICN was loaded inside a glove bag to avoid moisture and impurities from contaminating the sample. The matrix was deposited by introducing into the vacuum chamber a mixture of ICN, H_2O and Ar. The deposition rate was ~ 2 mmol/hr of the matrix gas. The experiments were performed using a double jet nozzle; through one nozzle ICN was introduced, while through the second nozzle, we introduced H_2O/Ar mixture. During deposition ICN was maintained at a temperature of -20^{0}C using a slush bath of alcohol and liquid nitrogen, to ensure a sufficiently low vapour pressure, to avoid multimer formation in the matrix. H_2O to Ar ratio was maintained at 1:1000. Spectra of precursors (ICN and water) were also recorded individually for comparison. After depositing a matrix which typically lasted about an hour, the FTIR spectrum of the deposited sample in the matrix, was recorded. After recording the spectrum the temperature of the matrix was raised to 32 K, maintained at this temperature for half an hour, and then re-cooled to 12K. The FTIR spectrum of the annealed matrix was the recorded. Annealing was performed to encourage diffusion of the deposited species so that intermolecular complexes could be formed.

4.1.3 Experimental Features for the ICN⋯H_2O Complex

The FTIR spectrum of ICN-H_2O co-deposited and annealed is shown in Fig. 1. Spectra of ICN and H_2O individually deposited is also shown. On annealing the matrix where ICN-H_2O was co-deposited, new features were observed that were not seen when either ICN or H_2O were individually deposited. These new features must be due to the complex, between ICN and water. The shift in these features due to the complex, from those of the monomer feature is indicative of the nature of the complex. These features are assigned by comparing them with those obtained from computations. For a comparison of computational and experimental features, the computed features were appropriately scaled. Scaling factor for a particular region in the spectrum is calculated by dividing the experimental wavenumber for the monomer feature by the computed wavenumber for the same mode of the monomer. This factor is then used to scale the computed features of the complex for comparison with the experimental features.

4.1.3.1 C≡N Stretch Region

Figure 10: Experimental spectra over the spectral regions of 2190-2160 cm^{-1}
A: Water, B: ICN, C: ICN-Water complex (x:1:1000) at 12K, D: spectrum after annealing.
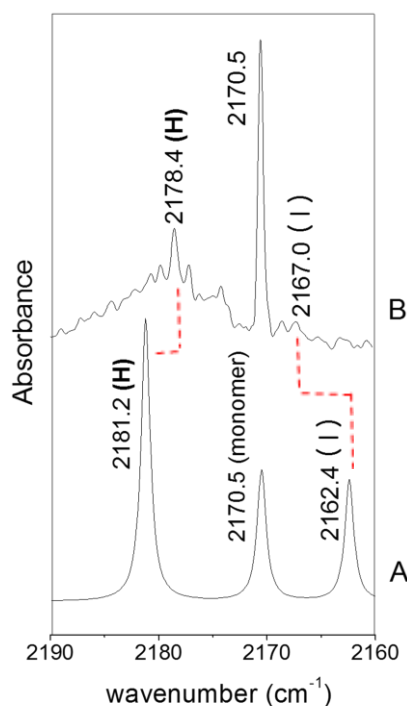
Figure 11: Computed (A) and Experimental [annealed] (B) spectrum of ICN-Water complex (x:1:1000) over the spectral regions of 2190-2160 wavenumbers.

Matrix isolation FTIR spectra of ICN, water and complex in the CN stretch region is shown in Fig 10 and comparison between the experimental and computed spectra is shown in Fig 11. The C≡N stretch of ICN occurs at 2170.5 cm^{-1}. On co-deposition of the two precursors and annealing, a red shifted feature at 2167.0 cm^{-1} was observed which is due to the complex. This feature is assigned to the CN stretching frequency in the Iodine bonded complex, since the computed feature corresponding to this interaction is also indicated to be red shifted. The scaling factor for this region is 0.922. A broad feature at 2178.4 cm^{-1} which is a blue shifted

feature relative to the ICN feature, is assigned to the C≡N stretch in hydrogen bonded complex. Computations also indicate the CN stretch to be blue shifted in the hydrogen bonded complex. This feature is present in the spectrum obtained when ICN also was deposited, since H_2O is an ubiquitous impurity in any matrix isolation experiment. However, that this feature is due to the ICN-H_2O hydrogen bonded complex is confirmed based on the absorption that when water was deliberately added, the intensity of this feature increases.

4.1.3.2   O-H Stretch Region
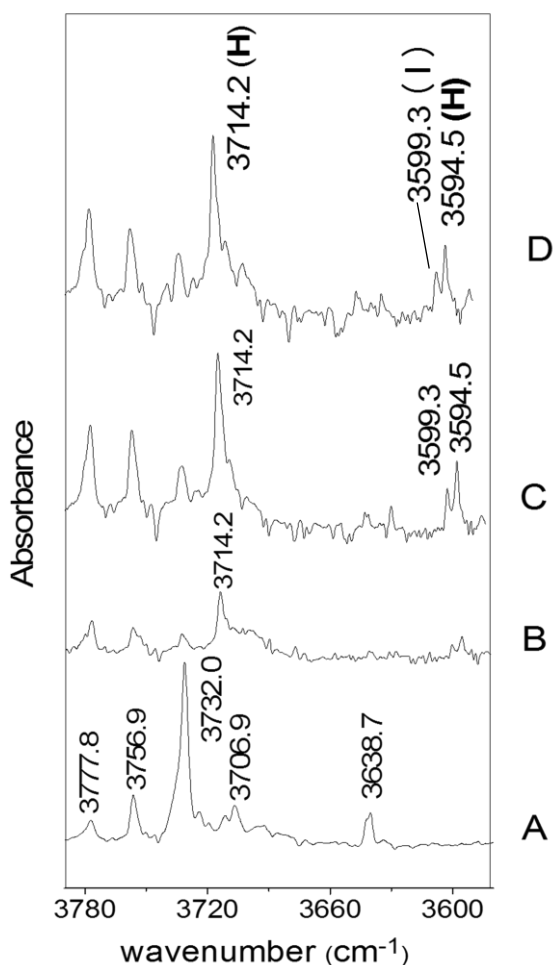
Figure 12: Experimental spectra showing the O-H tretch region
A: Water, B: ICN, C: ICN-Water complex (x:1:1000) at 12K, D: spectrum after annealing
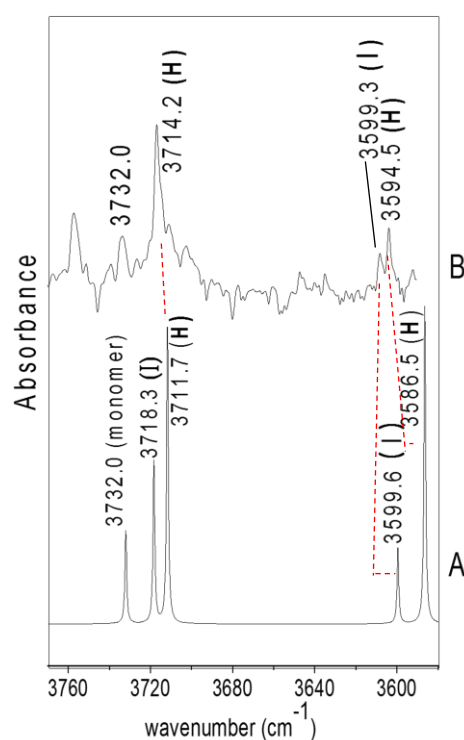
Figure 13: Computed (A) and Experimental [annealed] (B) spectrum of ICN-Water complex (x:1:1000) showing the O-H stretch region

Matrix isolation FTIR spectra of ICN, water and complex in the OH stretch region is shown in Fig 12 and comparison between the experimental and computed spectra is shown in

Fig 13. The feature for antisymmetric stretch of water comes at 3732.0 cm^{-1}. The scaling factor for this region was calculated to be 0.94. Calculations show that for both iodine bonding and halogen bonding interactions, OH antisymmetric stretch is red shifted with hydrogen bonded structure being more intense. In the experimental spectrum a broad and intense feature was observed at 3714.2 cm^{-1}, which was not present in the monomer spectrum. This feature is assigned to the hydrogen bonded complex based on its intensity. Since the peak is broad at the base, it is possible that the halogen bonded feature, which is of less intensity is unresolved. In the computed spectrum, the features corresponding to both the interactions are only separated by a few wavenumbers.

For the symmetric stretch of water, also two blue shifted features, separated by 5 wavenumbers were observed. Based on the relative intensity of halogen bonded and hydrogen bonded features in the computed spectrum, the peak at 3594.5 cm^{-1} is assigned to the hydrogen bonding interaction and that at 3599.3 cm^{-1} is assigned to the halogen bonding interaction.

Table 3 shows the experimental and computed wavenumbers for both the interactions. Values given in brackets are the shifts in wavenumbers of complex features from monomer features. A negative value corresponds to redshift in wavenumber and a positive value corresponds to blue shift in wavenumber.

Table 3: Experimental and scaled computed wavenumbers of monomer and complex features (shifts in parenthesis)

Experimental wavenumbers (cm^{-1})			Computed wavenumbers (cm^{-1}) [scaled]			Mode Assignment
Monomer	Iodine bonding	Hydrogen bonding	Monomer	Iodine bonding	Hydrogen bonding	
2170.5	2167.0 (-3.5)	2178.4 (7.9)	2170.5	2162.4 (-8.1)	2181.2 (10.7)	CN stretch
3732.0	-	3714.2 (-17.8)	3732.0	3718.3 (-13.7)	3711.7 (-20.3)	OH antisymmetric stretch
3638.7	3599.3 (-39.4)	3594.5 (-44.2)	3604.4	3599.6 (-4.8)	3586.5 (-17.9)	OH symmetric stretch

4.1.4 NBO Analysis

Having established that ICN can interact with water through iodine bond and hydrogen bond, NBO analysis was performed to discern the donor and acceptor orbitals involved in these interactions and the extent of their interaction. Table 4 shows the donor and acceptor orbitals

in each interaction, delocalization energy (E_2), energy difference between the orbitals [E(j)-E(i)] and the off diagonal element of Fock matrix (F_{ij}) for each of the interactions.

The NBO analysis shows that when a halogen bond is formed the lone pair of electron of oxygen is getting donated to the C-I σ^* orbital of ICN whereas the lone pair of nitrogen of ICN goes to the O-H σ^* orbital of water in case of hydrogen bonding. The extent of these interactions are given by the delocalization energies. The delocalization energy for halogen bonding is more than that of the hydrogen bonding. This could be a plausible explanation for the halogen bonded complex being the global minimum.

Table 4: NBO data for the two types of non-covalent interactions in the ICN-water complex

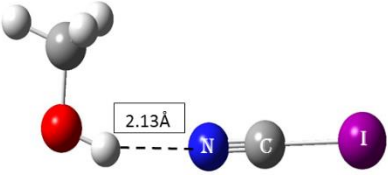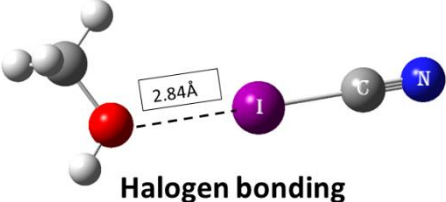| ICN-water Complex	Donor NBO	Acceptor NBO	E_2(kcal/mol)	E(j)-E(i) [a.u.]	F_{ij} [a.u.]
Halogen bonding	L.P. of O	C-I (σ^*)	6.04	0.87	0.065
Hydrogen bonding	L.P. of N	O-H (σ^*)	5.76	1.24	0.076

4.2   ICN-METHANOL COMPLEXES

To confirm that what we are observing is right and systematic, interaction of ICN with methanol was studied. The advantage of choosing this system is that, along with the shifts in C≡N and O-H stretching features one can also look at the shifts in C-O stretch of methanol for signatures corresponding to different non-covalent interactions. Quantum chemical calculations were performed using Gaussian 09 suite of programmes. The different isomers of ICN⋯Methanol at the MO6-2X/DGDZVP level of theory are given below along with the Raw, ZPE and BSSE corrected stabilization energies of the complex in table 5.

It can be seen that three types of non-covalent interactions are shown in this system; a halogen bonded complex involving an I⋯O interaction, a classical hydrogen bonded interaction between N of ICN and H or H_2O. In addition, there was also a carbon bonded complex, which can be manifested as a C⋯O interaction. Of these isomers, the halogen bonded isomer is the most strongly bound complex, with a BSSE corrected interaction energy of -7.8 kcal/mol. The hydrogen bonded complex was next in stability with a BSSE corrected interaction energy of -4.0 kcal/mol. The carbon bonded complex also had an interaction energy similar to the hydrogen bonded complex. The iodine bonded complex is the global minimum on the potential energy surface. In the halogen bonded isomer, I⋯O bond length is 2.84 Å and the C-I-O angle

is nearly equal to 180^0. In the hydrogen bonded complex N$\cdots$H bond length is equal to 2.13 Å and N-H-O angle is equal to 156^0.

Table 5: Optimized geometries of ICN-methanol system and the interaction energies of complexes

Isomer	Interaction Energy Raw/ZPE/BSSE (kcalmol^{-1})
Hydrogen bonding	-4.9/-3.9/-4.0
Halogen bonding	-8.4/-7.7/-7.8

4.2.1 AIM Analysis

The charge density topology of molecules was studied by applying the AIM theory by Bader to the optimized geometries. Using the theory bond critical points (3,-1) associated with the complexes were located. The structures obtained at the M06-2X/DGDZVP level of theory are shown in fig. 14. The bond critical points corresponding to the halogen and hydrogen bonds have been circled.
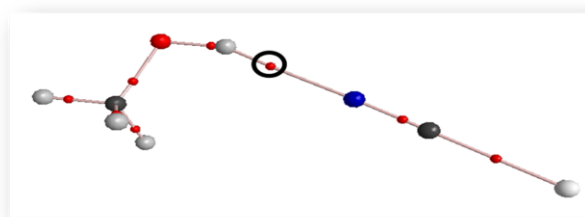
Hydrogen bonded complex
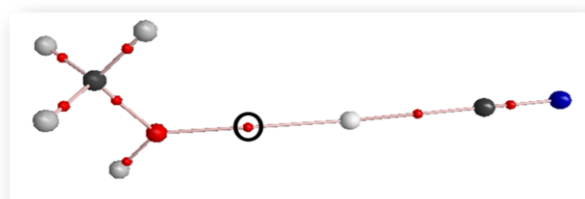
Halogen bonded complex

Figure 14: Structures of the complex showing bond critical points at the M06-2X/DGDZVP level of theory

Also, electron density ρ(r) and Laplacian of electron density were computed for the critical points associated with the non-covalent interactions under consideration, the values of which are given in table 6.

Table 6: AIM data for the different isomers of ICN-methanol complex

Isomer	Charge density at b.c.p. ρ(r)	Laplacian of ρ(r) at b.c.p.
Halogen bonded complex	0.020 a.u.	0.073 a.u.
Hydrogen bonded complex	0.018 a.u.	0.068 a.u.

The values of ρ(r) and Laplacian of ρ(r) at bond critical points are in good agreement with the values given in literature for halogen bonding and hydrogen bonding.

Frequency calculations were also performed at the MO6-2X/DGDZVP level of theory. The vibrational frequencies corresponding to different normal modes of the optimized structures were calculated. All the vibrational frequencies were positive confirming that the obtained geometries are minima on the potential energy surface.

4.2.2 Experimental

ICN was loaded inside a glove bag to avoid moisture and impurities from contaminating the sample. The matrix was deposited by introducing into the vacuum chamber a mixture of ICN, methanol and Ar. The deposition rate was ~ 2 mmol/hr of the matrix gas. The experiments were performed using a double jet nozzle; through one nozzle ICN was introduced, while through the second nozzle, we introduced Methanol/Ar mixture. During deposition ICN was maintained at a temperature of -20^{0}C using a slush bath of alcohol and liquid nitrogen, to ensure a sufficiently low vapour pressure, to avoid multimer formation in the matrix. Methanol to Ar ratio was maintained at 1:1000. Spectra of precursors (ICN and methanol) were also recorded individually for comparison. After depositing a matrix which typically lasted about an hour, the FTIR spectrum of the deposited sample in the matrix, was recorded. After recording the spectrum the temperature of the matrix was raised to 32 K, maintained at this temperature for half an hour, and then re-cooled to 12K. The FTIR spectrum of the annealed matrix was the recorded. Annealing was performed to encourage diffusion of the deposited species so that intermolecular complexes could be formed.

4.2.3 Experimental Features for the ICN···Methanol Complex

4.2.3.1   C-O Stretch Region
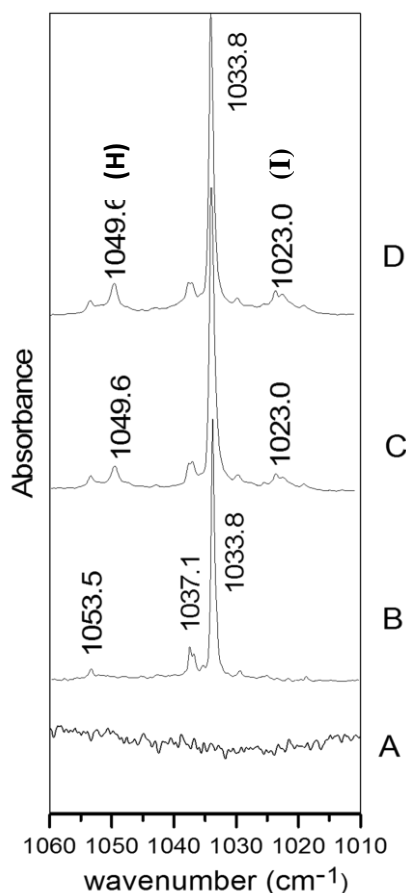
Figure 15: Experimental spectra over the spectral regions of 1060-1010 cm⁻¹
A: ICN, B: Methanol, C: ICN-Methanol complex (x:1:1000) at 12K, D: spectrum after annealing.
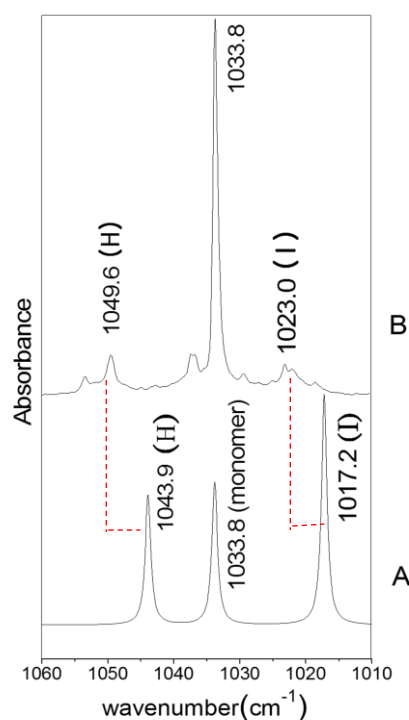
Figure 16: Computed (A) and Experimental [annealed] (B) spectrum of ICN-Methanol complex (x:1:1000) over the spectral regions of 2190-2160 wavenumbers.

Matrix isolation FTIR spectra of ICN, methanol and complex in the CO stretch region is shown in Fig 15 and comparison between the experimental and computed spectra is shown in Fig 16. The CO stretch of methanol occurs at 1033.8 cm⁻¹. On co-deposition of the two precursors and annealing, a red shifted feature at 1023.0 cm⁻¹ was observed which is due to the complex. This feature is assigned to the CO stretching frequency in the Iodine bonded complex, since the computed feature corresponding to this interaction is also indicated to be red shifted.

The scaling factor for this region is 0.920. A feature at 1049.6 cm^{-1} which is a blue shifted feature relative to the monomer (methanol) feature is assigned to the CO stretch in the hydrogen bonded complex. Computations also indicate the CO stretch to be blue shifted in the hydrogen bonded complex. The CO stretch region of methanol gives conclusive evidence for the presence of halogen bonding and hydrogen bonding interaction in ICN-Methanol complex.

4.2.3.2   C≡N Stretch Region
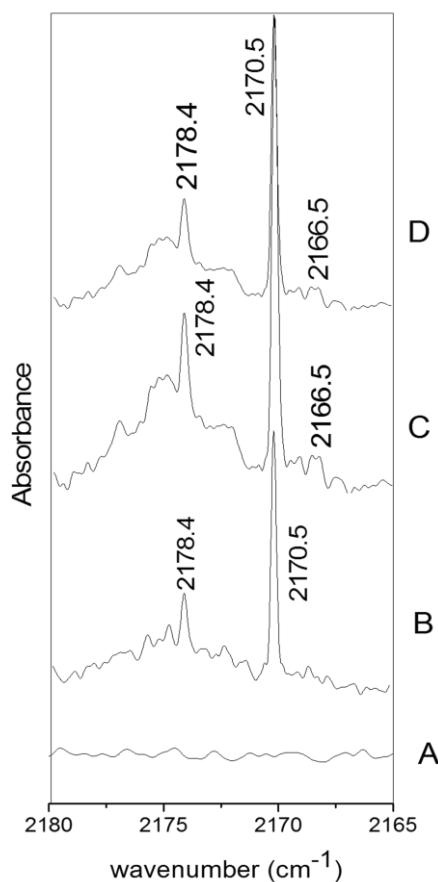
Figure 17: Experimental spectra showing the C≡N stretch region
A: Methanol, B: ICN, C: ICN-Methanol complex (x:1:1000) at 12K, D: spectrum after annealing.

Figure 18: Computed (A) and Experimental [annealed] (B) spectrum of ICN-Methanol complex (x:1:1000) showing the C≡N stretch region.
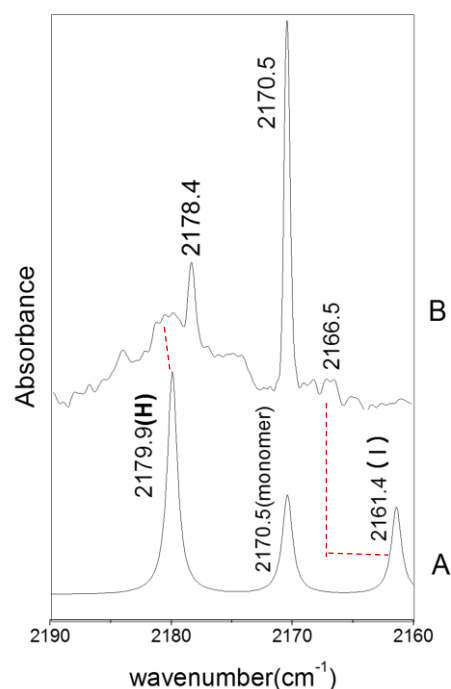
Matrix isolation FTIR spectra of ICN, methanol and complex in the CN stretch region is shown in Fig 17 and comparison between the experimental and computed spectra is shown in Fig 18. The C≡N stretch of ICN occurs at 2170.5 cm^{-1}. On codepostion of the two precursors and annealing, a red shifted feature at 2166.5 cm^{-1} was observed which is due to the complex. This feature is assigned to the CN stretching frequency in the Iodine bonded complex, since the computed feature corresponding to this interaction is also indicated to be red shifted. The

scaling factor for this region is 0.922. Calculations indicate the CN stretch to be blue shifted in the hydrogen bonded complex. The broad feature at 2178.4 cm^{-1} is due to the C≡N stretch in hydrogen bonded complex of ICN-water since H_2O is an ubiquitous impurity in any matrix isolation experiment. However, when methanol is present, a hump is seen on the broad feature which could be due to the ICN-methanol hydrogen bond.

4.2.3.3   O-H Stretch Region

**Figure 19: Experimental spectra showing the O-H stretch region
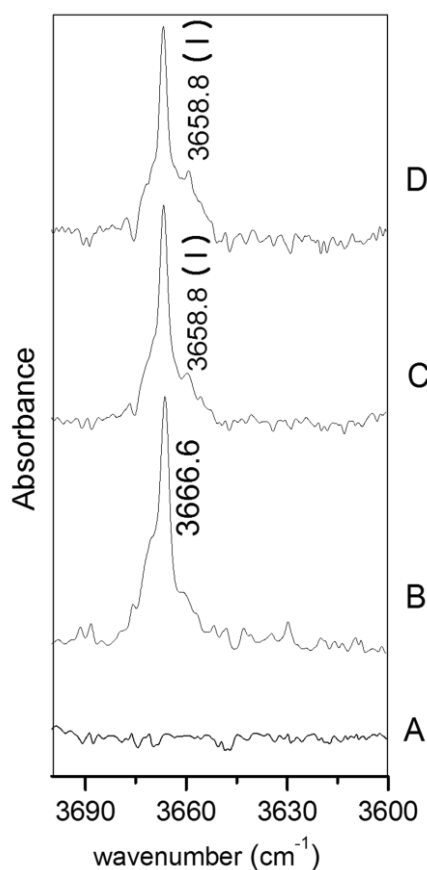A: ICN, B: Methanol, C: ICN-Methanol complex (x:1:1000) at 12K, D: spectrum after annealing**

Figure 20: Computed (A) and Experimental [annealed] (B) spectrum of ICN-Methanol complex (x:1:1000) showing the O-H stretch region
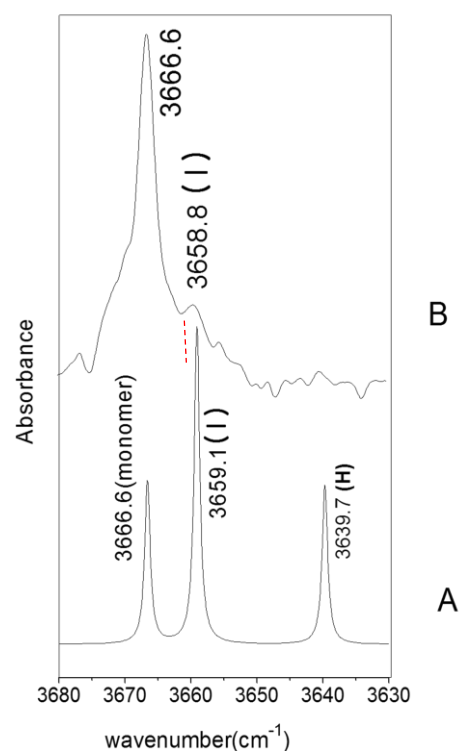
Matrix isolation FTIR spectra of ICN, methanol and complex in the OH stretch region is shown in Fig 19 and comparison between the experimental and computed spectra is shown in Fig 20. The feature for OH stretch of methanol comes at 3666.6 cm^{-1}. The scaling factor for this region was calculated to be 0.947. Calculations show that for both iodine bonding and halogen bonding interactions, OH astretch is red shifted with iodine bonded structure being more intense. In the experimental spectrum a new feature was observed at 3658.8 cm^{-1}, which

was not present in the monomer spectrum. This feature is assigned to the iodine bonded complex, since the computed feature corresponding to this interaction also gives similar shift. Signatures for hydrogen bonded complex was not observed in this region. Calculations show that the intensity of peak corresponding to the hydrgen bonded complex is less than the peak corresponding to the halogen bonded complex, which could be the reason for not observing features for hydrogen bonding in the spectrum.

Table 7 shows the experimental and computed wavenumbers for both the interactions. Values given in brackets are the shifts in wavenumbers of complex features from monomer features. A negative value corresponds to red shift in wavenumber and a positive value corresponds to blue shift in wavenumber.

Table 7: Experimental and scaled computed wavenumbers of monomer and complex features (shifts in parenthesis)

Experimental wavenumber (cm^{-1})			Computed wavenumber (cm^{-1}) [scaled]			Mode assignment
Monomer	I-bonded	H-bonded	Monomer	I-bonded	H-bonded	
1033.8	1023.0 (-10.8)	1049.6 (15.8)	1033.8	1017.2 (-16.6)	1043.9 (10.1)	CO stretch
2170.5	2166.5 (-4.0)	Broad feature	2170.5	2161.4 (-9.1)	2179.9 (9.4)	CN stretch
3666. 6	3658.8 (-7.8)	-	3666.6	3659.1 (-7.5)	3639.7 (-26.9)	OH stretch

4.2.4 NBO Analysis

Our matrix isolation infrared spectroscopy studies confirmed that ICN can interact with methanol through iodine bond and hydrogen bond. To discern the donor and acceptor orbitals involved in these interactions and the extent of their interaction, an NBO analysis was performed. Table 8 shows the donor and acceptor orbitals in each interaction, delocalization energy (E_2), energy difference between the orbitals [E(j)-E(i)] and the off diagonal element of Fock matrix (F_{ij}) for each of the interactions.

Table 8: NBO data for the two types of non-covalent interactions in the ICN-Methanol complex

| ICN-Methanol Complex	Donor NBO	Acceptor NBO	E_2(kcal/mol)	E(j)-E(i) [a.u.]	F_{ij} [a.u.]
Halogen bonding	L.P. of O	C-I (σ*)	4.71	0.72	0.052
	L.P. of O	C-I (σ*)	2.74	0.66	0.038
Hydrogen bonding	L.P. of N	O-H (σ*)	5.88	1.24	0.077

The NBO analysis shows that when a halogen bond is formed between methanol and ICN, lone pairs of electrons of oxygen are getting donated to the C-I σ* orbital of ICN whereas the lone pair of nitrogen of ICN goes to the O-H σ* orbital of water in case of hydrogen bonding. The extent of these interactions are given by the delocalization energies. The total delocalization energy for halogen bonding is the sum of delocalization energies for two individual interactions stabilizing the bonding. It is more than the delocalization energy for hydrogen bonding. Therefore, halogen bonding is the more stable interaction.

4.3 CARBON BONDED ISOMERS

Our experiments confirmed the presence of halogen bonding and hydrogen bonding interactions in ICN-water and ICN-methanol complexes. But calculations also showed the presence of a third type of bonding in these complexes, which is the carbon bonded complex which can be manifested as a C···O bond The optimized geometries and interaction energies (raw/BSSE/ZPE corrected) for ICN-water and ICN-methanol carbon bonded isomers are given below (Fig. 21).
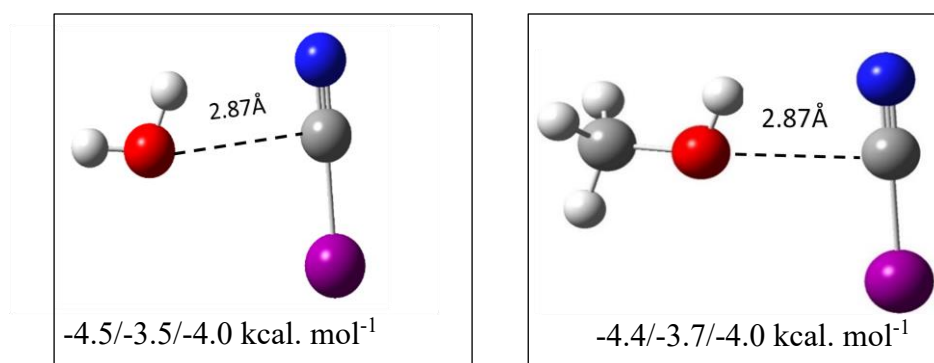
Figure 21: Carbon bonded isomers of ICN-Water and ICN-Methanol complexes and their interaction energies
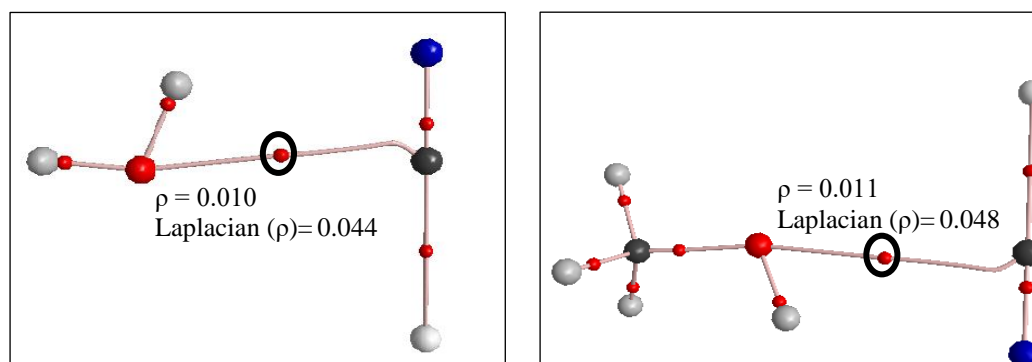
Figure 22: Structures of the complex showing bond critical points at the M06-2X/DGDZVP level of theory

The interaction energies of the carbon bonded structures are similar to that of the hydrogen bonded isomer in both ICN-water and ICN-methanol complexes. In the carbon bonded isomer of ICN-water, C$\cdots$O bond length is 2.87 Å. In the hydrogen bonded complex N$\cdots$H bond length is equal to 2.87 Å.

The charge density topology of molecules was studied by applying the AIM theory by Bader to the optimized geometries. Using the theory bond critical points (3,-1) associated with the complexes were located. The structures obtained at the M06-2X/DGDZVP level of theory are shown in fig. 22. The bond critical points corresponding to the carbon bonding is have been circled. Since we do not have experimental evidence to confirm the presence of this interaction, this interaction is proposed only on the basis of a computational study.

CONCLUSIONS

This study helped us to identify three different types of non-covalent interactions in ICN-water and ICN-methanol complexes: a halogen bonded complex involving an I···O interaction, a classical hydrogen bonded interaction between N of ICN and H of H_2O or methanol. In addition, there was also a carbon bonded complex, which can be manifested as a C···O interaction. Of these isomers, the halogen bonded isomer is the most strongly bound complex. The hydrogen bonded complex was next in stability. The carbon bonded complex also had an interaction energy similar to the hydrogen bonded complex. Our experiments conducted in argon matrix gave evidence for the formation of halogen bonded isomers and hydrogen bonded isomers in the matrix. The observed experimental wavenumbers were corroborated with the computations performed at M06-2X/DGDZVP level of theory. The carbon bonded isomer was not observed experimentally.

On co-deposition of the precursors and annealing, new features were observed in the spectrum due to the complex formation. In the CN stretching region of ICN and in the OH stretching region of water, signatures for hydrogen bonded and halogen bonded isomers were observed. The ICN-methanol experiments have provided evidence for the existence of I···O and N···H interactions through reasonable shifts in the CO stretch of methanol. More concentration dependent experiments are to be performed to confirm the presence of carbon bonded isomers of ICN-methanol and ICN-water complexes in matrix.

BIBLIOGRAPHY

(1)   Arunan, E.; Desiraju, G. R.; Klein, R. A.; Sadlej, J.; Scheiner, S.; Alkorta, I.; Clary, D. C.; Crabtree, R. H.; Dannenberg, J. J.; Hobza, P.; et al. Definition of the Hydrogen Bond (IUPAC Recommendations 2011). *Pure Appl. Chem.* **2011**, *83* (8), 1637–1641.

(2)   Desiraju, G. R.; Ho, P. S.; Kloo, L.; Legon, A. C.; Marquardt, R.; Metrangolo, P.; Politzer, P.; Resnati, G.; Rissanen, K. Definition of the Halogen Bond (IUPAC Recommendations 2013). *Pure Appl. Chem.* **2013**, *85* (8), 1711–1713.

(3)   Valadares, N. F.; Salum, L. B.; Polikarpov, I.; Andricopulo, A. D.; Garratt, R. C. Role of Halogen Bonds in Thyroid Hormone Receptor Selectivity: Pharmacophore-Based 3d-Qssr Studies. *J. Chem. Inf. Model.* **2009**, *49* (11), 2606–2616.

(4)   Clark, T.; Hennemann, M.; Murray, J. S.; Politzer, P. Halogen Bonding: The σ-Hole: Proceedings of "Modeling Interactions in Biomolecules II", Prague, September 5th-9th, 2005. *J. Mol. Model.* **2007**, *13* (2), 291–296.

(5)   Aakeröy, C. B.; Fasulo, M.; Schultheiss, N.; Desper, J.; Moore, C. Structural Competition between Hydrogen Bonds and Halogen Bonds. *J. Am. Chem. Soc.* **2007**, *129* (45), 13772–13773.

(6)   Geboes, Y.; De Proft, F.; Herrebout, W. A. Effect of Fluorination on the Competition of Halogen Bonding and Hydrogen Bonding: Complexes of Fluoroiodomethane with Dimethyl Ether and Trimethylamine. *J. Phys. Chem. A* **2017**, *121* (21), 4180–4188.

(7)   Martí-Rujas, J.; Colombo, L.; Lü, J.; Dey, A.; Terraneo, G.; Metrangolo, P.; Pilati, T.; Resnati, G. Hydrogen and Halogen Bonding Drive the Orthogonal Self-Assembly of an Organic Framework Possessing 2D Channels. *Chem. Commun.* **2012**, *48* (66), 8207.

(8)   Zhu, S.; Xing, C.; Xu, W.; Jin, G.; Li, Z. Halogen Bonding and Hydrogen Bonding Coexist in Driving Self-Assembly Process. *Cryst. Growth Des.* **2004**, *4* (1), 53–56.

(9)   Masoodi, H. R.; Bagheri, S.; Ranjbar, M. Theoretical Study of Cooperativity between Hydrogen Bond–hydrogen Bond, Halogen Bond–halogen Bond and Hydrogen Bond–halogen Bond in Ternary FX…diazine…XF (X = H and Cl) Complexes. *Mol. Phys.*

2016, *114* (23), 3464–3474.

(10)   Li, Q.; Xu, X.; Liu, T.; Jing, B.; Li, W.; Cheng, J.; Gong, B.; Sun, J. Competition between Hydrogen Bond and Halogen Bond in Complexes of Formaldehyde with Hypohalous Acids. *Phys. Chem. Chem. Phys.* **2010**, *12* (25), 6837.

(11)   Zhao, Q.; Feng, D.; Hao, J. The Cooperativity between Hydrogen and Halogen Bond in the XY•••HNC•••XY (X, y = F, Cl, Br) Complexes. *J. Mol. Model.* **2011**, *17* (11), 2817–2823.

(12)   Mani, D.; Arunan, E. The X–C⋯Y (X = O/F, Y = O/S/F/Cl/Br/N/P) 'Carbon Bond' and Hydrophobic Interactions. *Phys. Chem. Chem. Phys.* **2013**, *15* (34), 14377.

(13)   Bundhun, A.; Ramasami, P.; Murray, J. S.; Politzer, P. Trends in σ-Hole Strengths and Interactions of F3MX Molecules (M = C, Si, Ge and X = F, Cl, Br, I). *J. Mol. Model.* **2013**, *19* (7), 2739–2746.

(14)   Van Thiel, M.; Becker, E. D.; Pimentel, G. C. Infrared Studies of Hydrogen Bonding of Water by the Matrix Isolation Technique. *J. Chem. Phys.* **1957**, *27* (2), 486–490.

(15)   Whittle, E.; Dows, D. A.; Pimentel, G. C. Matrix Isolation Method for the Experimental Study of Unstable Species. *J. Chem. Phys.* **1954**, *22* (11), 1943–1943.

(16)   Bouteiller, Y.; Behrouz, H. Basis Set Superposition Error Effects on Electronic and ν $_{FX}$, ν $_{F⋯N}$ Stretching Modes of Hydrogen Bonded Systems FX⋯NCX (X=H,D). *J. Chem. Phys.* **1992**, *96* (8), 6033–6038.

(17)   Salvador, P.; Szczęśniak, M. M. Counterpoise-Corrected Geometries and Harmonic Frequencies of N-Body Clusters: Application to (HF)n(N=3,4). *J. Chem. Phys.* **2003**, *118* (2), 537–549.

(18)   Koch, U.; Popelier, P. L. A. Characterization of C-H-O Hydrogen Bonds on the Basis of the Charge Density. *J. Phys. Chem.* **1995**, *99* (24), 9747–9754.

(19)   Raghavendra, B.; Arunan, E. Unpaired and σ Bond Electrons as H, Cl, and Li Bond Acceptors: An Anomalous One-Electron Blue-Shifting Chlorine Bond. *J. Phys. Chem. A* **2007**, *111* (39), 9699–9706.

(20)   Gaussian 09, Revision A.1, M. J. Frisch, G. W. Trucks, H. B. Schlegel, G. E. Scuseria, M. A. Robb, J. R. Cheeseman, G. Scalmani, V. Barone, G. A. Petersson, H. Nakatsuji, X. Li,

M. Caricato, A. Marenich, J. Bloino, B. G. Janesko, R. Gomperts, B. Mennucci, H. P. Hratchian, J. V. Ortiz, A. F. Izmaylov, J. L. Sonnenberg, D. Williams-Young, F. Ding, F. Lipparini, F. Egidi, J. Goings, B. Peng, A. Petrone, T. Henderson, D. Ranasinghe, V. G. Zakrzewski, J. Gao, N. Rega, G. Zheng, W. Liang, M. Hada, M. Ehara, K. Toyota, R. Fukuda, J. Hasegawa, M. Ishida, T. Nakajima, Y. Honda, O. Kitao, H. Nakai, T. Vreven, K. Throssell, J. A. Montgomery, Jr., J. E. Peralta, F. Ogliaro, M. Bearpark, J. J. Heyd, E. Brothers, K. N. Kudin, V. N. Staroverov, T. Keith, R. Kobayashi, J. Normand, K. Raghavachari, A. Rendell, J. C. Burant, S. S. Iyengar, J. Tomasi, M. Cossi, J. M. Millam, M. Klene, C. Adamo, R. Cammi, J. W. Ochterski, R. L. Martin, K. Morokuma, O. Farkas, J. B. Foresman, and D. J. Fox, Gaussian, Inc., Wallingford CT, 2016.

(21) Friedrich Biegler-Konig, Jens Schonbohm, and R. F. W. Bader. AIM 2000 version 2.37,2002.